OPTICAL REVIEW Vol. 15, No. 1 (2008) 51–56

Depth-Adaptive Regularized Reconstruction for Reflection Diffuse Optical Tomography

Reiko ENDOH*, Mamiko FUJII, and Kiyoshi NAKAYAMA†

Department of Electrical and Electronics Engineering, Faculty of Science and Technology, Sophia University, Tokyo 102-8554, Japan

(Received May 15, 2007; Accepted June 13, 2007)

We study reflection diffuse optical tomography using two-dimensional (2D) continuous-wave source-detector arrays on the surface of semi-infinite medium, aiming at imaging the perfusion and the hemoglobin oxygen saturation variation of human cerebral cortex with brain activation. We had previously formulated the inverse problem with Moore–Penrose inversion. When we use simple regularization in this inverse problem, the reconstruction sensitivity decreases markedly with the depth so that the signal in the deep range may be masked by an unwanted signal in the shallow range. In this paper, we propose a depth-adaptive regularized reconstruction, in which we assign a smaller regularization parameter with the depth. We demonstrate improvement of the three-dimensional (3D) reconstruction uniformity using the proposed scheme.

Key words: diffuse optical tomography, DOT, 3D image reconstruction, depth-adaptive regularized reconstruction, inverse problem, regularization parameter, brain activity measurement

1. Introduction

In recent years there have been many theoretical and experimental reports on near-infrared (NIR) devices, which measure the perfusion and hemoglobin oxygen saturation variation of the human cerebral cortex with brain activation in real-time and visualize the local activated area as a two-dimensional (2D) topographic image.[1,2] These devices measure continuous diffused light by source detector pairs arranged on the head.

Meanwhile, numerous studies concerning three-dimensional (3D) image reconstruction in diffuse optical tomography (DOT) have also been reported. Most of these studies are aimed at obtaining a cross-sectional image of oxygenation and require information concerning photon path length to discriminate strong scattering effects on the reconstructed image.[3–5] Typically used methods include the so-called time-domain or frequency domain technique with a surrounding optode arrangement. These techniques are suitable for achieving high quality imaging in diffuse optical imaging, however, measurements are large-scale, costly and time consuming. Therefore, NIR devices of continuous wave (CW) source type with a 2D source-detector arrangement still have features for many potential applications. However, these devices do not have depth resolution, and cannot discriminate blood volume change of the cerebral cortex with brain activity or change on the skin blood volume with autonomic nerve activity.

We have been studying diffuse optical tomography which has 3D spatial resolution using 2D CW source-detector arrays, aiming at real time imaging of the brain activation not contaminated by the skin circulation fluctuation. Our approach is to realize 3D spatial resolution with 2D CW source-detector arrays by an inverse problem method. Pogue *et al.* successfully introduced depth-adaptive regularization in the DOT for the circular bounded plane region.[3] This, however, is on the weighted back projection in the iterative process to solve a nonlinear problem, which is far more intractable than the problem we addressed. Several research groups also reported the image reconstruction in DOT using the Moore–Penrose generalized inverse,[6] but in a recent paper one of these groups stated that they failed to reconstruct the target at the depth correct position.[7]

In our previous studies, we had formulated the forward problem based on the Rytov approximation, for the small perturbation of absorption coefficients in the diffusion equation approximation of photon migration, and formulated 3D tomographic reconstruction using simple regularized Moore–Penrose pseudo-inverse.[8,9] We had demonstrated feasibility of the 3D image reconstruction, and analyzed the trade-off between the reconstruction error and the spatial resolution and their depth dependencies.[9–11] In this report, we address the problem of the uniformity of image reconstruction for reflection diffuse optical tomography which has the features of unconstraint, real-time imaging and moderate cost. One of the difficulties of this type of tomography arises from the strong spatial non-uniformity of the measurement sensitivity. Namely, since the source-detector arrays are on the surface, the measured data have much larger sensitivity on the inhomogeneity in the shallow region than in the deeper region. Consequently, since the Moore–Penrose inverse seeks the minimum norm solution, large data sensitivity in the shallow region is reflected on the large sensitivity of the reconstruction of the inhomogeneity in the shallow region. Thus, in the simple regularized Moore–Penrose inversion studied so far, the inhomogeneity signal in the shallow region tends to mask the inhomogeneity signal in the deeper region. This tendency should be mitigated because we are interested in the brain activation rather than the skin circulation. In this article, we propose a

*Present affiliation: Research Center for Medical Sciences, The Jikei University School of Medicine.
†Present affiliation: Electro Design Corporation.

depth-adaptive regularization scheme, in which we assign the smaller regularization parameter to the deeper range so as to realize uniform reconstruction sensitivity with the depth.

2. Method

2.1 Forward problem

All the simulations were based on the diffusion equation approximation with extrapolated zero-boundary condition.[12] We consider the case in which absorption coefficient μ_a is spatially varying while scattering coefficient μ_s' is homogeneous. Using Rytov approximation for small perturbations of absorption coefficient, the perturbed fluence rate $\Phi(\boldsymbol{r}_s, \boldsymbol{r}_d)$ at the detector position $\boldsymbol{r}_d$ with the source position at $\boldsymbol{r}_s$ is expressed as[13]

$$\Phi(\boldsymbol{r}_s, \boldsymbol{r}_d) = \Phi_0(\boldsymbol{r}_s, \boldsymbol{r}_d) \exp[\Phi_{pert}(\boldsymbol{r}_s, \boldsymbol{r}_d)]. \quad (1)$$

Φ_0 is the unperturbed fluence rate for the baseline optical properties. Φ_{pert} is the perturbation caused by absorption coefficient change and is represented as[13]

$$\Phi_{pert}(\boldsymbol{r}_s, \boldsymbol{r}_d) = -\Phi_0(\boldsymbol{r}_s, \boldsymbol{r}_d)^{-1} \int \frac{\delta\mu_a(\boldsymbol{r})}{D} \Phi_0(\boldsymbol{r}_s, \boldsymbol{r}) G(\boldsymbol{r}, \boldsymbol{r}_d)\, d\boldsymbol{r}^3. \quad (2)$$

$D = 1/(3\mu_s')$ is the diffusion coefficient, G is the Green function, and $\delta\mu_a$ is the small perturbation of absorption coefficient. The detector output $X(\boldsymbol{r}_s, \boldsymbol{r}_d)$ can be expressed as

$$X(\boldsymbol{r}_s, \boldsymbol{r}_d) = K\Phi(\boldsymbol{r}_s, \boldsymbol{r}_d), \quad (3)$$

where K is nominal system gain including source intensity, detector aperture etc. Here we implicitly assume that the source is unit impulse, then $\Phi_0(\boldsymbol{r}_s, \boldsymbol{r}_d) = G(\boldsymbol{r}_s, \boldsymbol{r}_d)$. We consider the detector output normalized by the nominal detector output for the baseline medium and take its logarithm as the measured data, which is

$$\ln\left[\frac{X(\boldsymbol{r}_s, \boldsymbol{r}_d)}{K\Phi_0(\boldsymbol{r}_s, \boldsymbol{r}_d)}\right] = \Phi_{pert}(\boldsymbol{r}_s, \boldsymbol{r}_d). \quad (4)$$

Moreover, if the spatial variation of μ_a is assumed to be piecewise-constant in the region of interest, integral of eq. (2) is discretized into the summation,

$$\Phi_{pert}(\boldsymbol{r}_s, \boldsymbol{r}_d) = -\sum_j \frac{\delta\mu_{a,j}}{D} G(\boldsymbol{r}_s, \boldsymbol{r}_d)^{-1} \int_{V_j} G(\boldsymbol{r}_s, \boldsymbol{r}) G(\boldsymbol{r}, \boldsymbol{r}_d)\, dV, \quad (5)$$

where $\delta\mu_{a,j}$ is the perturbation of the absorption coefficient of j-th voxel, and V_j designates the volume of j-th voxel. Accordingly, in the i-th measurement with the source position $\boldsymbol{r}_{s,i}$ and the detector position $\boldsymbol{r}_{d,i}$, the measured data eq. (4) is expressed as,

$$b_i = \sum_j A_{i,j} x_j, \quad (6)$$

where

$$A_{i,j} = -\frac{\mu_{a0}}{D} G(\boldsymbol{r}_{s,i}, \boldsymbol{r}_{d,i})^{-1} \int_{V_j} G(\boldsymbol{r}_{s,i}, \boldsymbol{r}_j) G(\boldsymbol{r}_j, \boldsymbol{r}_{d,i})\, dV, \quad (7)$$

and

$$x_j = \frac{\delta\mu_{a,j}}{\mu_{a0}}. \quad (8)$$

In matrix form eq. (7) is,

$$\boldsymbol{A}\boldsymbol{x} = \boldsymbol{b}. \quad (9)$$

2.2 Inverse problem

We estimate the absorption coefficient change from the measurement data using the Moore–Penrose inversion of eq. (9). This inversion satisfies three properties, 1) reflexive, 2) minimum norm, and 3) least error. In an underdetermined problem like our case, the minimum norm is the most relevant feature. Because of this property, the large elements of the matrix $\boldsymbol{A}$ for an unknown tend to result in a large value of the inverse solution for that unknown.

Usually, an inverse problem is ill-posed, which leads to oscillatory solutions. To suppress the instability of the solution, people use the simple regularized Moore–Penrose inversion,

$$\boldsymbol{x}' = \boldsymbol{A}^T(\boldsymbol{A}\boldsymbol{A}^T + \lambda\boldsymbol{I})^{-1}\boldsymbol{b}, \quad (10a)$$

or

$$\boldsymbol{x}' = (\boldsymbol{A}^T\boldsymbol{A} + \lambda\boldsymbol{I})^{-1}\boldsymbol{A}^T\boldsymbol{b}, \quad (10b)$$

where $\boldsymbol{I}$ is identity matrix and λ is the Tikhonov regularization parameter. Equation (10a) is usually used for an underdetermined problem to lessen computational load, although eqs. (10a) and (10b) give exactly the same solution.[14,15] These simple regularizations, however, do not change the minimum norm nature of the solution. We are to mitigate the minimum norm nature by replacing the identity matrix in eq. (10b) with a diagonal matrix whose diagonal elements are positive. In most research of eq. (10a) has been utilized, because a variant regularization of this type can modify the weighting of the measurement data according to the S/N, but it cannot improve the inappropriate reconstruction of the target in the deep region.

In this paper, we propose a depth-adaptive regularization,

$$\boldsymbol{x}' = (\boldsymbol{A}^T\boldsymbol{A} + \boldsymbol{D}_\lambda)^{-1}\boldsymbol{A}^T\boldsymbol{b}, \quad (11)$$

where $\boldsymbol{D}_\lambda$ is a regularization diagonal matrix whose diagonal elements are chosen adaptively depending on the depth. As to the determination of regularization matrix $\boldsymbol{D}_\lambda$ which realizes uniform reconstruction sensitivity over the region of interest, we took the heuristic way (see Appendix). We determined the value of the diagonal elements of the regularization matrix simply proportional to the square-root of the corresponding diagonal elements of $\boldsymbol{A}^T\boldsymbol{A}$.

3. Simulation

Figure 1 shows our simulation model and its coordinate system. We assumed semi-infinite turbid medium at $z \geq 0$. The 4×4 CW source matrix spans $-5 \leq x, y \leq 15$ mm and 5×5 detector matrix spans $-20 \leq x, y \leq 20$ mm at the surface $z = 0$ mm. The region of interest spans $-21 \leq x, y \leq 21$ mm and $0 \leq z \leq 24$ mm, which is divided into uniform $14 \times 14 \times 8$ ($3 \times 3 \times 3\,\text{mm}^3$) voxels. The turbid medium

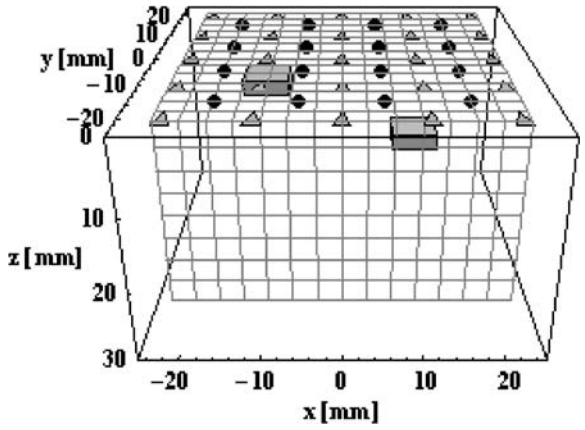

Fig. 1. Simulation model. Region of interest is divided into uniform $14 \times 14 \times 8$ $(3 \times 3 \times 3\,\mathrm{mm}^3)$ voxels. Circles denote source positions. Triangles denote detector positions.

was assigned with the baseline optical properties of $\mu'_{s0} = 1\,\mathrm{mm}^{-1}$ and $\mu_{a0} = 0.02\,\mathrm{mm}^{-1}$. We simulated two objects: one with $\mu'_s = 1\,\mathrm{mm}^{-1}$ and $\delta\mu_a = 0.01\,\mathrm{mm}^{-1}$ having dimensions $6 \times 6 \times 2\,\mathrm{mm}^3$ centered at $(x, y, z) = (-10, 0, 3)$ mm and the other at $(10, 0, 11)$ mm, simultaneously, representing the skin circulation change and the brain activity, respectively.

4. Results and Discussion

Figure 2 shows the x–z cross sectional images; a) is using simple regularization with $\lambda = 10^{-2}$, and b) is depth-adaptive regularization. In the depth-adaptive regularization, we assigned the diagonal elements values of the regularization matrix from $\lambda_1 = 5.25 \times 10^{-2}$ through $\lambda_{1568} = 3.40 \times 10^{-7}$, decreasing with the depth, proportional to the square-root of the corresponding diagonal elements of matrix $\boldsymbol{A}^{\mathrm{T}}\boldsymbol{A}$. In the simple regularization Fig. 2(a), the shallow target at the highly sensitive region is reconstructed much stronger than the deep target at the low sensitivity region. Moreover, both the shallow and deep reconstructed signals appear closer to the surface compared to the original position. The deep "wanted" target is reconstructed too shallow, and may be masked by the shallow unwanted signal. On the other hand, in Fig. 2(b) using depth-adaptive regularization, the deep wanted target is reconstructed at the correct position and is intensified compared with that using simple regularization. This clearly demonstrates the improved reconstruction using the proposed scheme.

More quantitatively, Fig. 3 depicts the one-dimensional (1D) longitudinal profiles of reconstructed absorption coefficient change at $(x, y) = (-10, 0)$ and $(10, 0)$ mm, where the unwanted and the wanted object should be reconstructed, respectively. The peaks of the reconstructed absorption coefficient changes are shown to occur at the correct

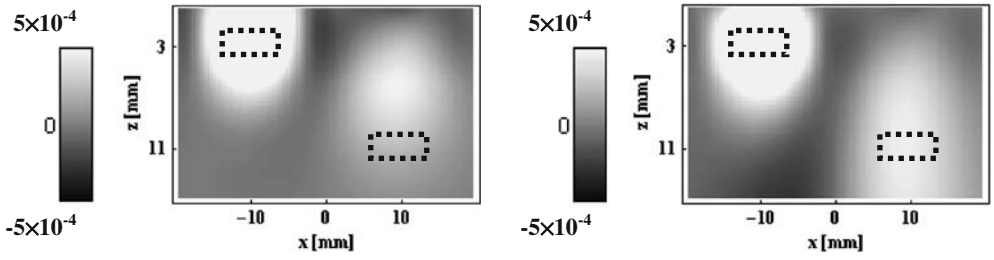

Fig. 2. The x–z cross sectional images at $y = 0$ mm (measurement $S_{0,\max}/N = 160$ dB). Gray scale is linear and ranges over -5×10^{-4} (black) $\leq \delta\mu_a \leq 5 \times 10^{-4}\,\mathrm{mm}^{-1}$ (white). Dotted rectangles indicate objects. (a) Simple and (b) depth-adaptive regularization.

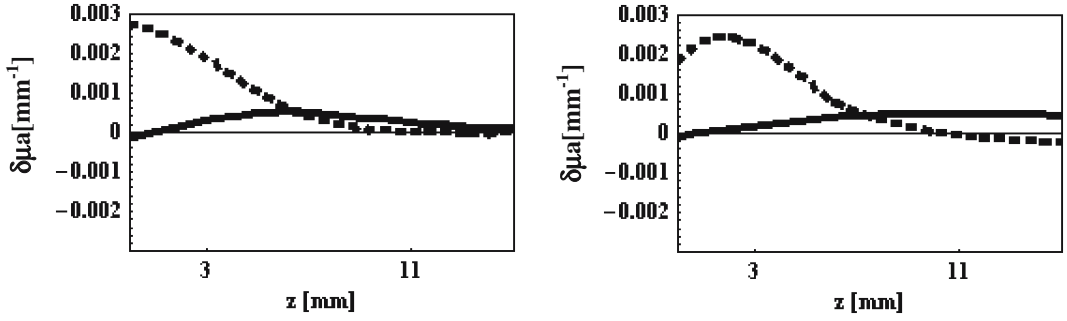

Fig. 3. 1D longitudinal profiles of reconstructed absorption coefficient change (measurement $S_{0,\max}/N = 160$ dB). Solid lines are at $x = 11$ mm and $y = 0$, and dotted lines are at $x = -10$ mm and $y = 0$. (a) Simple and (b) depth-adaptive regularization.

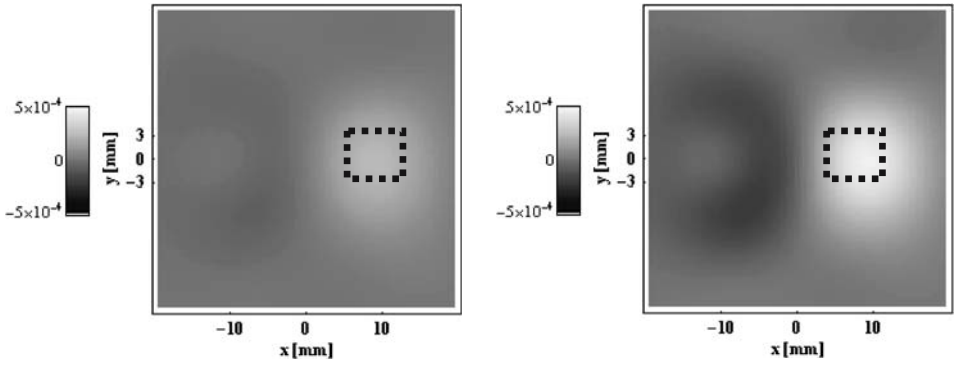

Fig. 4. The x–y plane images at $z = 11$ mm (measurement $S_{0,\max}/N = 160$ dB). Gray scale is linear and ranges over -5×10^{-4} (black) $\leq \delta\mu_a \leq 5 \times 10^{-4}\,\mathrm{mm}^{-1}$ (white). Dotted rectangles indicate objects. (a) Simple and (b) depth-adaptive regularization.

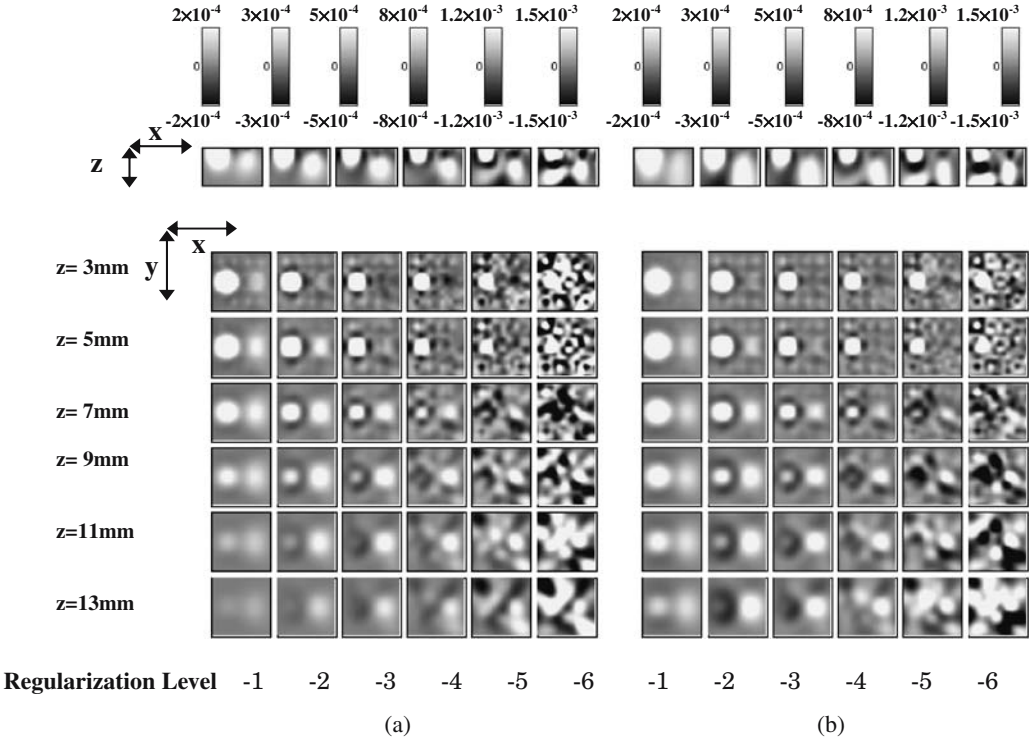

Fig. 5. Reconstructed images for various regularization levels (measurement $S_{0,\max}/N = 160$ dB). First row panels show x–z cross sectional images, and panels from second to seventh row show the x–y plan images at $z = 3$ to 13 mm. Gray scale is linear. (a) Simple and (b) depth-adaptive regularization.

positions of objects in (b) using the depth-adaptive regularization scheme, whereas (a) by simple regularization, target positions are clearly biased to the surface. Figure 4 shows the x–y plane images at $z = 11$ mm, where the wanted target should be reconstructed. In (a) by simple regularization, however, one cannot see any clear objects; On the other hand, we can clearly see only the wanted signal in (b) by depth-adaptive regularization. This is a practically important result, because in the actual brain activity measurement, those x–y plane images at the cerebral cortex surface would be used for the clinical examination.

Figure 5 shows images with various regularization levels. The regularization level $-n$ designates $\lambda = 10^{-n}$ for simple regularization and $\lambda_1 = 5.25 \times 10^{-n}$ through $\lambda_{1568} = 3.40 \times 10^{-5-n}$ decreasing with depth for depth-adaptive regularization. In the meantime, results already described in Fig. 2, Figs. 3 and 4 are the reconstruction of regularization level -2. In Fig. 5, column (a) shows the reconstruction by simple regularization and column (b) shows the reconstruction by the depth-adaptive regularization. In both types of regularization, one can see that the spatial resolution improves with the decreased regularization level but noise and the

signal instability also increase, so that one needs to determine the regularization level considering this trade-off. Figure 5 also demonstrates that the depth-adaptive regularization surpasses the simple regularization from the viewpoint of correctness of the reconstructed position of the target and the evenness of the reconstructed signal strength over wide-ranging regularization levels.

In the actual measurement, the measurement noise is primarily determined by the shot noise of the detector. If we presume a parallel measurement scheme with all the sources on, using frequency division modulation for sources, the shot noise is determined by $S_{0,\max}$, which is the baseline detector signal from the nearest source. From this standpoint, we have been using $S_{0,\max}/N$ to prescribe the noise condition. Apparently, $S_{0,\max}/N = 160$ or 140 dB needed for this particular simulation model seems unrealizable for the real-time measurement having an appropriate signal band width for the brain circulation change. The required $S_{0,\max}/N$ value, however, is very much dependent on the source-detector configurations and the region of interest. Also, if we incorporate a time division scheme in the measurement, the required S_0/N will be greatly reduced because we become concerned with the shot noise generated by the baseline signal from the second-nearest or third-nearest sources. All these practical considerations and designs are needed for actual realization of the reflection diffuse optical tomography for brain activity measurement.

5. Conclusion

We proposed a depth-adaptive regularization scheme to improve the uniformity of the signal reconstruction sensitivity in reflection diffuse optical tomography. Through the simulation of two objects representing skin circulation change and brain activation, we demonstrated the improvement of uniformity of the 3D reconstructed image using the proposed scheme. We were able to reconstruct the wanted target in the deep region at the correct position without its being masked by the shallow unwanted signal.

Further study is needed on practical confinement of the region of interest, corresponding optimal arrangement of source-detectors and a data acquisition scheme to realize actual reflection diffuse optical tomography for brain activity measurement.

Acknowledgment

This work was partially supported by a Grant-in-Aid for Scientific Research (No. 15300169) from the Ministry of Education, Culture, Sports, Science and Technology.

Appendix

To investigate the minimum norm solution given by the Moore–Penrose inversion, we consider the simplest underdetermined problem, which has only one equation or data for two unknowns, $\boldsymbol{b} = \boldsymbol{A}\boldsymbol{x}$, where $\boldsymbol{b} = [b]$, $\boldsymbol{A} = [a_1, a_2]$, $\boldsymbol{x} = [x_1, x_2]^{\mathrm{T}}$, and $a_1, a_2, b > 0$.

Although all the points on the line $a_1x_1 + a_2x_2 = b$ are solutions, the Moore–Penrose inversion gives the minimum norm solution,

$$\boldsymbol{x}' = \boldsymbol{A}^{\mathrm{T}}(\boldsymbol{A}\boldsymbol{A}^{\mathrm{T}})^{-1}\boldsymbol{b} = \begin{bmatrix} \dfrac{a_1 b}{{a_1}^2 + {a_2}^2} & \dfrac{a_2 b}{{a_1}^2 + {a_2}^2} \end{bmatrix}. \tag{A·1}$$

If, for example, the forward weighting a_1 for unknown x_1 is larger than a_2 for x_2, we have larger backward weighting for the estimated x'_1, and the ratio of the estimated unknowns x'_1 and x'_2 is equal to the ratio of the forward weightings for the unknowns. This is the same as the solution by back-projection.

Generally, to suppress the instability of the solution, which is caused by the ill-posed nature of the inverse problem, people use the simple regularized Moore–Penrose inversion,

$$\boldsymbol{x}' = (\boldsymbol{A}^{\mathrm{T}}\boldsymbol{A} + \lambda \boldsymbol{I})^{-1}\boldsymbol{A}^{\mathrm{T}}\boldsymbol{b}, \tag{A·2}$$

where $\boldsymbol{I}$ is identity matrix and λ is the Tikhonov regularization parameter. Applying the simple regularization to the simplest problem, eq. (A·2) gives,

$$\boldsymbol{x}' = \left(\begin{bmatrix} {a_1}^2 & a_1 a_2 \\ a_1 a_2 & {a_2}^2 \end{bmatrix} + \begin{bmatrix} \lambda & 0 \\ 0 & \lambda \end{bmatrix} \right)^{-1} \begin{bmatrix} a_1 \\ a_2 \end{bmatrix} [b] = \begin{bmatrix} \dfrac{a_1 b}{{a_1}^2 + {a_2}^2 + \lambda} & \dfrac{a_2 b}{{a_1}^2 + {a_2}^2 + \lambda} \end{bmatrix}. \tag{A·3}$$

We note that the simple regularization has no essential change to minimum norm nature, because it only changes the common factor for two unknowns. We try to change the ratio of estimated unknowns by introducing a diagonal regularization matrix in place of the identity matrix,

$$\boldsymbol{x}' = (\boldsymbol{A}^{\mathrm{T}}\boldsymbol{A} + \boldsymbol{D}_\lambda)^{-1}\boldsymbol{A}^{\mathrm{T}}\boldsymbol{b}, \tag{A·4}$$

where $\boldsymbol{D}_\lambda$ is a diagonal regularization matrix whose diagonal elements are positive. The solution for the simplest problem is

$$\boldsymbol{x}' = \left(\begin{bmatrix} {a_1}^2 & a_1 a_2 \\ a_1 a_2 & {a_2}^2 \end{bmatrix} + \begin{bmatrix} \lambda_1 & 0 \\ 0 & \lambda_2 \end{bmatrix} \right)^{-1} \begin{bmatrix} a_1 \\ a_2 \end{bmatrix} [b] = \begin{bmatrix} \dfrac{a_1 \lambda_2}{{a_1}^2\lambda_2 + {a_2}^2\lambda_1 + \lambda_1\lambda_2} b & \dfrac{a_2 \lambda_1}{{a_1}^2\lambda_2 + {a_2}^2\lambda_1 + \lambda_1\lambda_2} b \end{bmatrix}. \tag{A·5}$$

As is seen from eq. (A·5), if we choose regularization parameters λ_1 and λ_2 proportional to the square-root of the corresponding diagonal elements of $\boldsymbol{A}^{\mathrm{T}}\boldsymbol{A}$, we would obtain equal weighting for two unknowns. By letting

$$\lambda_1 = \lambda\sqrt{{a_1}^2},\ \lambda_2 = \lambda\sqrt{{a_2}^2}, \tag{A·6}$$

eq. (A·5) becomes

$$\boldsymbol{x}' = \begin{bmatrix} \dfrac{b}{a_1 + a_2 + \lambda} & \dfrac{b}{a_1 + a_2 + \lambda} \end{bmatrix}, \tag{A·7}$$

which is an approximate solution having equal weighting for two unknowns.

In our problem, to realize the uniformity of the reconstructed signal sensitivity, we have to assign the smaller regularization parameter with the depth because the measurement signal sensitivity markedly decreases with the

depth. In practice, the depth-adaptive regularization parameters are determined proportional to the square-root values of corresponding diagonal elements of matrix $\boldsymbol{A}^{\mathrm{T}}\boldsymbol{A}$.

References

1) Hitachi Medical Corporation, Optical Tomography System: http://www.hitachi-medical.co.jp/opt-e
2) Shimadzu Corporation, NIRStation: http://www.med.shimadzu.co.jp/products/om/01.html
3) B. W. Pogue, T. O. McBride, J. Prewitt, U. L. Österberg, and K. D. Paulsen: Appl. Opt. **38** (1999) 2950.
4) F. Gao, Y. Tanikawa, H. Zhao, and Y. Yamada: Appl. Opt. **41** (2002) 7346.
5) Y. Xu, X. Gu, T. Khan, and H. Jiang: Appl. Opt. **41** (2002) 5427.
6) A. Li, E. L. Miller, M. E. Kilmer, T. J. Brukilacchio, T. Chaves, J. Stott, Q. Zhang, T. Wu, M. Chorlton, R. H. Moore, D. B. Kopans, and D. A. Boas: Appl. Opt. **42** (2003) 5181.
7) A. M. Dale and D. A. Boas: Appl. Opt. **44** (2005) 1957.
8) R. Endoh, A. Suzuki, M. Fujii, and K. Nakayama: Proc. Asian Symp. Biomedical Optics and Photomedicine, 2002, p. 60.
9) R. Endoh, M. Fujii, A. Suzuki, and K. Nakayama: Proc. IEEE EMBS Asian-Pacific Conf. Biomedical Engineering, 2003, p. 021286.
10) R. Endoh, A. Suzuki, M. Fujii, and K. Nakayama: Phys. Med. Biol. **49** (2004) 1881.
11) R. Endoh, A. Suzuki, M. Fujii, and K. Nakayama: Tech. Dig. OSA Biomedical Topical Meetings, 2004, p. 14.
12) R. C. Haskell, L. O. Svaasand, T. Tsay, T. Feng, M. S. McAdams, and B. J. Tromberg: J. Opt. Soc. Am. A **11** (1994) 2727.
13) M. A. O'Leary, D. A. Boas, B. Chance, and A. G. Yodh: Opt. Lett. **20** (1995) 426.
14) T. Musha and Y. Okamoto: *Gyaku-mondai-to Sono-tokikata* (Inverse Problems and Their Solutions) (Ohmusha, Tokyo, 1992) p. 127 [in Japanese].
15) A. Li, G. Boverman, Y. Zhang, D. Brooks, E. L. Miller, M. E. Kilmer, Q. Zhang, E. M. C. Hillman, and D. A. Boas: Appl. Opt. **44** (2005) 1948.